


Novel nonequilibrium steady states in multiple emulsions

Cite as: Phys. Fluids **32**, 017102 (2020); <https://doi.org/10.1063/1.5134901>

Submitted: 04 November 2019 . Accepted: 19 December 2019 . Published Online: 09 January 2020

A. Tiribocchi , A. Montessori, S. Aime, M. Milani, M. Lauricella , S. Succi , and D. Weitz 

COLLECTIONS

 This paper was selected as Featured



View Online



Export Citation



CrossMark

ARTICLES YOU MAY BE INTERESTED IN

[Characterizing three-dimensional features of vortex surfaces in the flow past a finite plate](#)
Physics of Fluids **32**, 011903 (2020); <https://doi.org/10.1063/1.5134551>

[Experimental study of hypersonic boundary layer transition on a permeable wall of a flared cone](#)

Physics of Fluids **32**, 011701 (2020); <https://doi.org/10.1063/1.5139546>

[Turbulent drag reduction by polymer additives: Fundamentals and recent advances](#)
Physics of Fluids **31**, 121302 (2019); <https://doi.org/10.1063/1.5129619>

Scilight Highlights of the best new research
in the **physical sciences**

[LEARN MORE!](#)



Novel nonequilibrium steady states in multiple emulsions

Cite as: Phys. Fluids 32, 017102 (2020); doi: 10.1063/1.5134901

Submitted: 4 November 2019 • Accepted: 19 December 2019 •

Published Online: 9 January 2020



A. Tiribocchi,^{1,2}  A. Montessori,² S. Aime,³ M. Milani,^{4,3} M. Lauricella,²  S. Succi,^{1,2,5}  and D. Weitz^{3,6} 

AFFILIATIONS

¹Center for Life Nano Science@La Sapienza, Istituto Italiano di Tecnologia, 00161 Roma, Italy

²Istituto per le Applicazioni del Calcolo CNR, via dei Taurini 19, Rome, Italy

³School of Engineering and Applied Sciences, Harvard University, McKay 517, Cambridge, Massachusetts 02138, USA

⁴Università degli Studi di Milano, via Celoria 16, 20133 Milano, Italy

⁵Institute for Applied Computational Science, John A. Paulson School of Engineering and Applied Sciences, Harvard University, Cambridge, Massachusetts 02138, USA

⁶Department of Physics, Harvard University, Cambridge, Massachusetts 02138, USA

ABSTRACT

We numerically investigate the rheological response of a noncoalescing multiple emulsion under a symmetric shear flow. We find that the dynamics significantly depends on the magnitude of the shear rate and on the number of the encapsulated droplets, two key parameters whose control is fundamental to accurately select the resulting nonequilibrium steady states. The double emulsion, for instance, attains a static steady state in which the external droplet stretches under flow and achieves an elliptical shape (closely resembling the one observed in a sheared isolated fluid droplet), while the internal one remains essentially unaffected. Novel nonequilibrium steady states arise in a multiple emulsion. Under low/moderate shear rates, for instance, the encapsulated droplets display a nontrivial planetarylike motion that considerably affects the shape of the external droplet. Some features of this dynamic behavior are partially captured by the Taylor deformation parameter and the stress tensor. Besides a theoretical interest on its own, our results can potentially stimulate further experiments, as most of the predictions could be tested in the lab by monitoring droplets' shapes and position over time.

Published under license by AIP Publishing. <https://doi.org/10.1063/1.5134901>

I. INTRODUCTION

A multiple emulsion is an intriguing example of soft material in which smaller drops of an immiscible fluid are dispersed within a larger one.^{1–8} A well-known example is the double emulsion in which, for instance, a water/oil emulsion is dispersed in a water-continuous phase.^{9–12} Higher complex systems are emulsions made of multidistinct inner cores (such as a triple W/O/W/O emulsion) and monodisperse or polydisperse droplets encapsulated in a larger one.^{13–16}

Due to their unique hierarchical structure, these systems are highly desirable in a wide number of applications, including drug delivery of chemical and biological compounds,^{11,17–22} triggered reaction and mixing,^{23–27} cell-based therapies,^{28–31} waste water treatment,^{32,33} cosmetics,^{1,34–38} and food science.^{27,39–42} Unlike rigid colloids, they possess additional shape flexibility, adjustable, for

instance, by carefully modulating the thickness and viscosity of the shell of fluid.^{43,44} This is a crucial requirement in many applications where a precise control of the rate of permeability, as well as on mechanical stability, is necessary.^{20,21,45}

Although inherently out of equilibrium, these systems can be stabilized by means of suitable surfactants adsorbed onto the droplet interfaces. Indeed, the design of a well-defined multiple emulsion, with the controlled size and number of secondary droplets, is fundamental for the correct functioning of devices in which inner droplets' coalescence or cross-contamination of their content must be avoided.^{46,47} In this context, it is crucial to investigate the dynamic behavior of the internal droplets, since their reciprocal interaction, mediated by the surfactant and by the surrounding fluid, may affect the rate of release of the cargo carried within as well as the stability of the entire emulsion.^{4,48} This is a must in high internal phase multiple emulsions (of interest in food science and cosmetics)

in which fluid interfaces occupy large portions of the system and long-range effects may dramatically affect functionality and design.^{49–52}

Besides their technological relevance, multiple emulsions hold a great theoretical interest, due to the capability of exhibiting nontrivial interface topologies associated with a complex hydrodynamics, especially when subject to an external flow field.^{53–55}

Yet, despite the impressive progress in production and design of encapsulated droplets, to date, their dynamics under an imposed flow has been only partially investigated. While significant efforts have been addressed to understand the rheological response of single phase droplets^{56–58} as well as of double emulsions,^{53,54,59–61} much less is known for higher complex systems, such as those reported in Fig. 1, which shows an example of a multiple emulsion with two and three cores fabricated in a microfluidic device.¹³ In the regime of low or moderate shear forces, for instance, the internal droplet of a double emulsion remains approximately spherical and motionless at the steady state, in contrast to the external one that attains a final ellipsoidal shape^{53,54} and may acquire motion. However, what is the scenario if two or more inner fluid droplets are included? More specifically, what is their dynamics under flow? Importantly, how do they affect the shape and stability of the external droplet?

In this work, we investigate, by means of lattice Boltzmann simulations, the dynamic response of a multicore emulsion under an externally imposed shear flow. The basic physics of this system is captured by a multiphase field continuum model,^{62,63} based on a Landau free-energy description of the equilibrium properties of immiscible fluids employed to compute the thermodynamic forces (pressure tensor and chemical potential) governing the time evolution of the system.⁶⁴

By varying the shear rate and the number of inner droplets, we observe new nonequilibrium steady states in which the encapsulated droplets showcase a persistent periodic planetarylike motion triggered by the fluid vorticity. Such dynamics is rather robust since it occurs regardless of the initial position of the internal droplets and of their volume fraction, as long as this is sufficiently far from

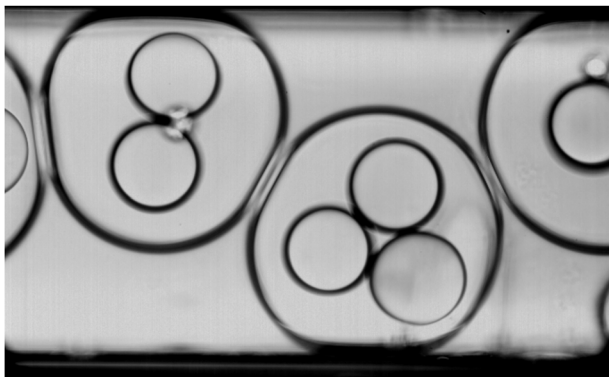


FIG. 1. Double emulsion with two and three cores, fabricated in a coflowing microfluidic device.¹³ Here, the continuous phase and the inner droplets are both water, whereas the middle phase is HFE 7500, a fluorinated oil. The interface is stabilized by adding 10% neat (undissolved) 008-FluoroSurfactant to the oil phase.

the close packing limit. Remarkably, this behavior leads to nontrivial modifications of the external droplet, whose steady-state shape significantly departs from the usual elliptical geometry, due to the presence of periodic local deformations occurring at its interface. These results suggest that the rheological response of a multiple emulsion is by far more complex than that of single or double emulsions, even in the regime where weak deformations are expected to occur.

The paper is organized as follows: In Sec. II, we describe the computational model used to simulate their rheological behavior, while in Sec. III, we show the main numerical results. We start by investigating the rheology of a single isolated fluid droplet, and afterwards, we elucidate the dynamics of a double emulsion under shear flow. Subsequently, we report the results on the nonequilibrium steady states observed in a multiple emulsion, in particular, when two and three fluid droplets are encapsulated. A discussion about the shape deformation and dynamic behavior of the external fluid interface is also provided. Finally, we conclude with some remarks and perspectives.

II. METHOD

A. Free energy and equations of motion

Here, we illustrate the physics and the modeling of a compound emulsion made of a suspension of immiscible fluid droplets encapsulated in a larger drop. Such droplets are described by using a multiphase field approach^{62,63,65} in which a set of scalar phase-field variables $\phi_i(\mathbf{r}, t)$, $i = 1, \dots, N$ (where N is the total number of droplets), accounts for the density of each droplet at position \mathbf{r} and time t , while a vector field $\mathbf{v}(\mathbf{r}, t)$ describes the underlying fluid velocity.

By assuming local equilibrium,⁶⁴ the properties of this mixture can be described by an effective coarse-grained free energy density

$$f = \frac{a}{4} \sum_i \phi_i^2 (\phi_i - \phi_0)^2 + \frac{k}{2} \sum_i (\nabla \phi_i)^2 + \epsilon \sum_{i,j,i < j} \phi_i \phi_j. \quad (1)$$

The first term is a double-well potential ensuring the existence of two coexisting minima: $\phi_i = \phi_0$ inside the i th droplet and 0 outside. The second term gauges the energetic cost associated with the droplet fluid interface. The parameters a and k are two positive constants controlling the interfacial thickness $\xi = 5\sqrt{k/2a}$ of each droplet and their surface tension $\sigma = \sqrt{8ak/9}$.^{66,67} The last term in Eq. (1) represents a soft-core repulsion whose strength is measured by the positive constant ϵ .

The dynamics of the order parameters $\phi_i(\mathbf{r}, t)$ is governed by a set of convection-diffusion equations

$$D_t \phi_i = -\nabla \cdot \mathbf{J}_i, \quad (2)$$

where $D_t = \partial/\partial t + \mathbf{v} \cdot \nabla$ is the material derivative and

$$\mathbf{J}_i = -M \nabla \mu_i \quad (3)$$

is the current, which is proportional to the product of the mobility M and the gradient of the chemical potential

$$\mu_i \equiv \frac{\delta \mathcal{F}}{\delta \phi_i} = \frac{\partial f}{\partial \phi_i} - \frac{\partial_\alpha f}{\partial (\partial_\alpha \phi_i)} \quad (4)$$

of the i th drop. Finally, $\mathcal{F} = \int_V f dV$ is the total free energy.

The fluid velocity $\mathbf{v}(\mathbf{r}, t)$ obeys the continuity and the Navier-Stokes equations, which, in the incompressible limit, are

$$\nabla \cdot \mathbf{v} = 0, \quad (5)$$

$$\rho \left(\frac{\partial}{\partial t} + \mathbf{v} \cdot \nabla \right) \mathbf{v} = \nabla \cdot \Pi. \quad (6)$$

In Eq. (6), ρ is the fluid density and Π is the total stress tensor given by the sum of three further terms. The first one is the isotropic pressure $\Pi^{is} = -p\delta_{\alpha\beta}$ and the second one is viscous stress $\Pi^{visc} = \eta(\partial_\alpha v_\beta + \partial_\beta v_\alpha)$, where η is the shear viscosity (Greek indices denote the Cartesian components). Finally, the last term takes into account interfacial contributions between different phases and is given by

$$\Pi^{inter} = \left(f - \sum_i \phi_i \frac{\delta \mathcal{F}}{\delta \phi_i} \right) \delta_{\alpha\beta} - \sum_i \frac{\partial \mathcal{F}}{\partial (\partial_\beta \phi_i)} \partial_\alpha \phi_i. \quad (7)$$

Note, in particular, that $\nabla \cdot \Pi^{inter} = -\sum_i \phi_i \nabla \mu_i$, representing the driving force due to the presence of spatially varying contributions of the order parameters.

B. Simulation details and numerical mapping

Equations (2), (5), and (6) are solved by using a hybrid numerical approach, in which the convection-diffusion equations are integrated by using a finite difference scheme while the continuity and the Navier-Stokes equations via a lattice Boltzmann algorithm.^{67–74} This method has been successfully adopted to simulate a wide variety of soft matter systems, ranging from binary fluids^{75–78} and liquid crystals^{79–83} to active gels,^{84,85} and has been recently extended to describe the physics of noncoalescing droplet suspensions.^{62,63}

All simulations are performed on two dimensional rectangular lattices (see Fig. 2) in order to minimize interference effects due to the periodic image of the droplets. These systems are sandwiched between two parallel flat walls placed at distance L_z , where we set no-slip conditions for the velocity field \mathbf{v} and neutral wetting for the fields ϕ_i . The former means that $v_z(z=0, z=L_z) = 0$, and the latter means that $\mathbf{n} \cdot \nabla \mu_i|_{z=0, L_z} = 0$ (no flux through the boundaries) and $\mathbf{n} \cdot \nabla (\nabla^2 \phi_i)|_{z=0, L_z} = 0$ (droplet interface perpendicular

at the boundaries), where \mathbf{n} is an inward normal unit vector at the boundaries.

In Fig. 2(a), an isolated isotropic fluid droplet (yellow) is initially placed at the center of the lattice and is surrounded by a second isotropic fluid (black). In this configuration, only one order parameter field ϕ is considered (i.e., $N = 1$). A double emulsion [Fig. 2(b)] is produced by means of two fields ϕ_i ($N = 2$). One is positive (equal to ≈ 2) within the smaller droplet (placed at the center of the lattice) and zero everywhere else, while the other one is positive outside the larger droplet and zero elsewhere. Analogous setups have been employed for the other multiple emulsion, when two ($N = 3$) and three ($N = 4$) droplets are included. The radii of the droplets have been chosen as follows: (a) $R = 30$, (b) $R_{in} = 10$ and $R_{out} = 30$, [(c) and (d)] $R_{in} = 15$ and $R_{out} = 56$. The corresponding emulsion volume fraction $V_f = \frac{N\pi R_{in}^2}{\pi R_{out}^2}$ is (a) $V_f = 0$, (b) $V_f \approx 0.11$, (c) $V_f \approx 0.15$, and (d) $V_f \approx 0.22$.

Starting from these initial conditions, the mixtures are first let to relax for $\approx 5 \times 10^3$ time steps to achieve a (near) equilibrium state. Afterwards, a symmetric shear is applied, by moving the top wall along the positive y -axis with velocity v_w and the bottom wall along the opposite direction with velocity $-v_w$. This sets a shear rate $\dot{\gamma} = 2v_w/L_z$. In our simulations, v_w ranges between 0.01 (low shear) and 0.05 (moderate/high shear), which means that $\dot{\gamma}$ varies between $\approx 2 \times 10^{-4}$ and $\approx 10^{-3}$ when $L_z = 110$ and between $\approx 1.1 \times 10^{-4}$ and $\approx 6 \times 10^{-4}$ when $L_z = 170$. As in previous works,⁵⁴ we define a dimensionless time $t^* = \dot{\gamma}(t - t_{eq})$, where t_{eq} is the relaxation time after which the shear is switched on. Unless otherwise explicitly stated, the following thermodynamic parameters have been used: $a = 0.07$, $M = 0.1$, $\eta = 1.67$, $k = 0.1$, and $\epsilon = 0.05$. In addition, throughout our simulations, time step and lattice spacing are fixed to unit value, $\Delta x = 1$, $\Delta t = 1$.

By following previous studies,^{62,63} an approximate mapping between simulation units and physical ones can be obtained by assuming a droplet of diameter roughly equal to $10^2 \mu\text{m}$ immersed in a background fluid of viscosity $\approx 10^{-2} \text{ Pa s}$ (assumed, for simplicity, equal to the viscosity of the fluid inside the droplet) and in which the surface tension σ , equal to ≈ 0.08 (for $k = 0.1$) in simulations, corresponds to $\sim 0.5\text{--}1 \text{ mN/m}$. With these parameters, a speed of 10^{-3} in simulation units corresponds to approximately 1 mm/s in real values. Further details are reported in the Appendix. A dimensionless quantity capturing droplet deformation is the capillary number $Ca = \frac{v\eta}{\sigma}$, measuring the strength of the viscous forces relative to the

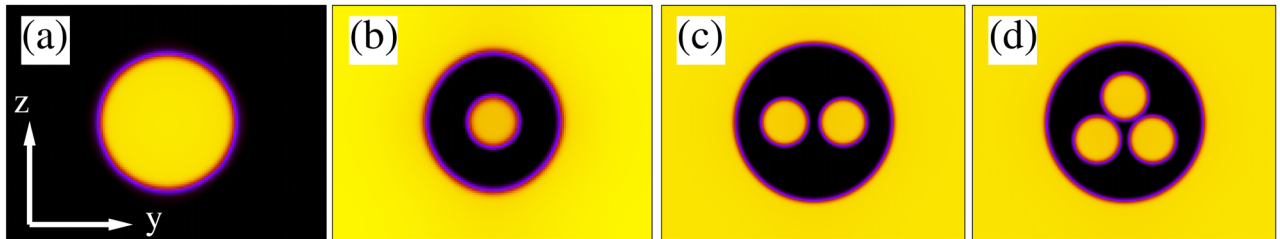


FIG. 2. Equilibrium profiles of different emulsions. (a) Isolated droplet, (b) double emulsion, (c) two-core multiple emulsion, and (d) three-core multiple emulsion. Lattice dimensions are [(a) and (b)] $L_y = 150$, $L_z = 110$; and [(c) and (d)] $L_y = 220$, $L_z = 170$. Droplet radii are (a) $R = 30$; (b) $R_{in} = 10$, $R_{out} = 30$; (c) $R_{in} = 15$, $R_{out} = 56$; and (d) $R_{in} = 15$, $R_{out} = 56$. Colors correspond to the values of the order parameter ϕ , ranging from 0 (black) to ≈ 2 (yellow).

surface tension. If, for example, $v = 0.01$, $Ca \sim 0.2$ (with $k = 0.1$). In addition, the Reynolds number $Re = \rho v_{max} L / \eta$ (where L is the system size and v_{max} is the maximum speed measured) may vary from ~ 1 to ~ 10 , the latter describing a regime for which inertial forces are much higher than the viscous ones and the condition of laminar flow is generally not fulfilled.

III. RESULTS

Here, we discuss the rheological response of the emulsions shown in Fig. 2 subject to a symmetric shear flow. To validate our model, we initially investigate the dynamics of an isolated fluid droplet and afterwards we move on to study the dynamical response of the other compound emulsions.

A. Isolated fluid droplet

As a first benchmark test, we simulate the effect produced by a symmetric shear flow to an isolated fluid droplet surrounded by a second immiscible fluid. A well-known result is that, for low/moderate values of $\dot{\gamma}$, at the steady state, the droplet attains an elliptical shape and aligns along the imposed shear flow. In Figs. 3(a) and 3(b) (Multimedia view), we show the steady state of the droplet and the corresponding fluid flow profile after imposing a shear rate $\dot{\gamma} \approx 1.8 \times 10^{-4}$. As expected, the droplet elongates and the major axis tilts and forms an angle of $\theta \approx 30^\circ$ with the shear direction. This is in very good agreement with the values reported in the literature for $Re \approx 2$ (see, for example, Ref. 57). The velocity field exhibits the typical structure observed for such a system, i.e., it is large and unidirectional near both walls and weaker in the center of the lattice, where a clockwise recirculation emerges within the droplet. The droplet position is mildly affected by the shear flow (see Fig. 4), which only slightly pushes the droplet rightwards with respect to the initial location.

As long as the droplet shape remains rather well-defined (like an ellipse), one can quantify its deformation in terms of the Taylor parameter $D = \frac{a-b}{a+b}$, where a and b represent the length of the major and the minor axis, respectively. It ranges between 0 (no deformation) and 1 (“needle” shape). In Fig. 4, it is shown that D attains a steady state value of ~ 0.18 , in line with experimental values observed when $Ca \sim 0.2$.^{56,86}

For higher values of $\dot{\gamma}$ (but low enough to avoid the droplet breakup⁸⁷), the droplet, once more, aligns with the flow direction and attains the elliptical shape but with a higher deformation at the steady state. If, for example, $\dot{\gamma} \approx 10^{-3}$, one gets $\theta \approx 40^\circ$ and $D \approx 0.65$,

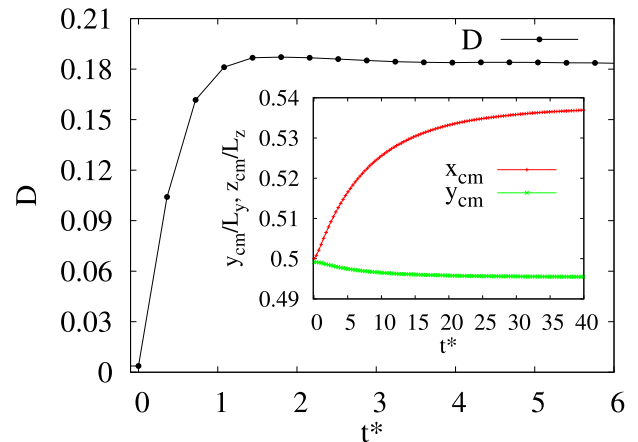


FIG. 4. Time evolution of the Taylor parameter D . Inset: Time evolution of the y and z components of the droplet center of mass. They are defined as $y_{cm}(t) = \frac{\sum_y y(t) \phi(y, z, t)}{\sum_y \phi(y, z, t)}$ and $z_{cm}(t) = \frac{\sum_z z(t) \phi(y, z, t)}{\sum_z \phi(y, z, t)}$, where $y = 1, \dots, L_y$, $z = 1, \dots, L_z$, and $\phi(y, z, t) \geq 0.1$.

values close to the experimental ones for $Re \approx 10^{57}$ [see movie MS “(Multimedia view)” in [supplementary material](#)].

These preliminary numerical tests reproduce with very good accuracy some aspects of the dynamic response under shear of an isolated fluid droplet. In Sec. III B, we extend this study to a Newtonian double emulsion in which a second droplet is included within a larger one.

B. Double emulsion

Due to the presence of an inner droplet, more complex hydrodynamics and interfacial deformations are expected with respect to the single-phase case. The effect of a moderate shear flow ($\dot{\gamma} \approx 1.8 \times 10^{-4}$) on a double emulsion is shown in Figs. 5(a) and 5(b) (Multimedia view). After the shear is imposed, the outer droplet is, once more, slightly advected rightwards (see Fig. 6, left) and, simultaneously, tilted and stretched along the shear direction until the elliptical steady-state shape is attained at approximately $t^* \approx 100$.

Here, we measure $\theta_o \approx 42^\circ$ and $D_o \approx 0.2$ (Fig. 6, right, green plot), values comparable with those of the single phase droplet. Hence, as long as $\dot{\gamma}$ is sufficiently small, the presence of the inner fluid droplet has a mild effect on the outer one, whose interface acts as an effective “shield” preventing deformations of the former.

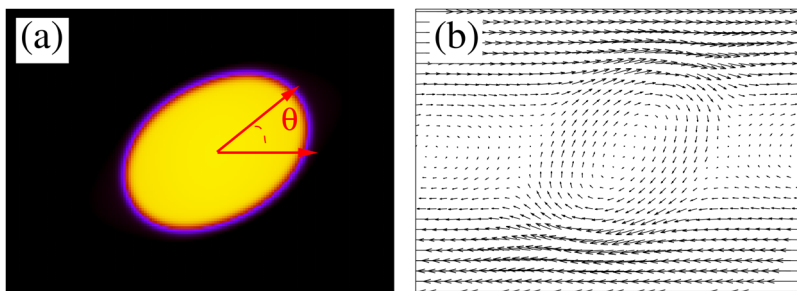


FIG. 3. (a) Steady state profile of an isolated droplet immersed in a second immiscible fluid subject to a symmetric shear flow with $\dot{\gamma} \approx 1.8 \times 10^{-4}$. In addition, $Re \approx 2$, $Ca \approx 0.21$, and $k = 0.1$. The angle θ indicates the direction of the droplet major axis with the shear flow. The color map is the same as that of Fig. 2. (b) Steady state velocity profile under shear. Intense opposite unidirectional flows are produced near the walls, whereas a much weaker fluid recirculation is observed within the droplet. Multimedia view: <https://doi.org/10.1063/1.5134901.1>

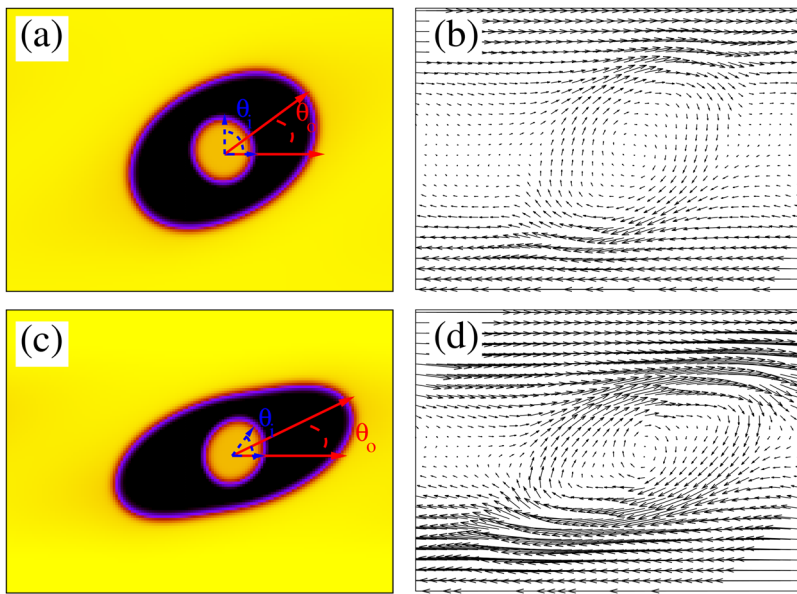


FIG. 5. [(a)–(c)] Steady state profiles of a double emulsion under a symmetric shear flow with (a) $\dot{\gamma} \approx 1.8 \times 10^{-4}$ and (c) $\dot{\gamma} \approx 4.5 \times 10^{-4}$. Here, $Re \approx 2$, $Ca \approx 0.21$ in (a) and $Re \approx 4.5$, $Ca \approx 0.52$ in (c). [(b)–(d)] Steady state velocity profiles under shear. Multimedia views: (a) and (c): <https://doi.org/10.1063/1.5134901.2>; (b) and (d): <https://doi.org/10.1063/1.5134901.3>

Indeed, the shape of the internal droplet remains almost unaltered throughout the process (we measure $\theta_i \approx 85^\circ$ and $D_i \approx 0.03$, see Fig. 6, right). This is mainly due to the large interfacial tension (higher than that of the outer droplet) induced by the small curvature radius, thus preventing deformations that would be favored by the shear flow. A further source of shape stabilization stems from the (weak) vorticity formed within the smaller droplet [in addition to the larger one mainly located in the layer between the droplets, see Fig. 5(b)], an effect known to inhibit deformations produced by the shear stress.^{88,89}

Doubling the shear rate can produce substantial shape deformations of the inner droplet as well as of the outer one. In Figs. 5(c) and 5(d) (Multimedia view), we show the steady state of a double emulsion when $\dot{\gamma} \approx 4.5 \times 10^{-4}$. Here, we got $\theta_o \approx 30^\circ$ and $\theta_i \approx 40^\circ$, while $D_i \approx 0.1$ and $D_o \approx 0.4$ (Fig. 6, right). Once again, due to its higher surface tension, the inner droplet is less deformed than the outer one, but, unlike the previous case, a visible rounded

clockwise recirculation, clearly distinct from the large elliptical one, forms inside.

Note that increasing $\dot{\gamma}$ produces a temporary peak in D , soon after the shear force is switched on. While, for low values of the shear rate, droplet elongation and alignment to the flow direction occurs gradually, for high values, it stretches rather abruptly and later on relaxes toward its steady state shape. As also observed in previous works,^{53,54} this initial deformation overshoot is necessary to overcome the additional inertia displayed by the droplet after an intense stretching.

Despite its comparatively simple design, the double emulsion displays a nontrivial rheological behavior, in which interface deformations and shape changes crucially depend on the elasticity and on the complex structure of the fluid velocity.

A largely unexplored physics is that of higher complex multiple emulsions, in which, for instance, two (or more) smaller fluid droplets are included within a larger external one. Section III C is

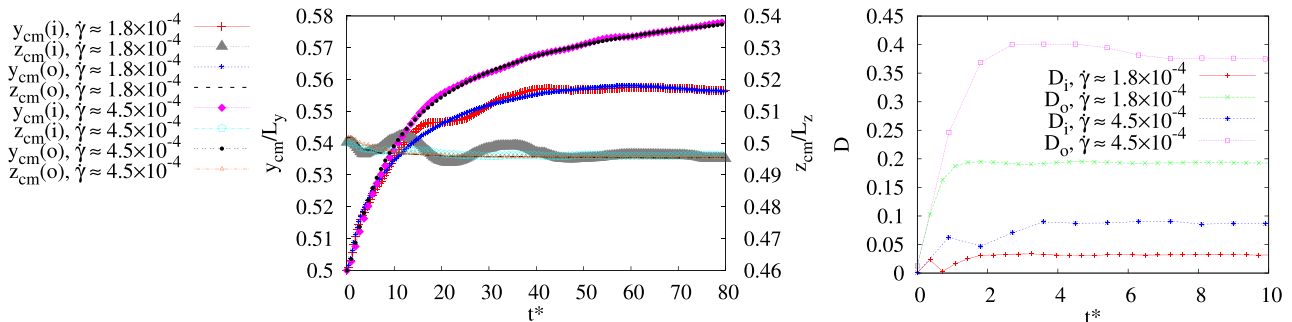


FIG. 6. (Left) Time evolution of the y and z components of the droplet centers for mass in the double emulsion for two different values of $\dot{\gamma}$. In both cases, the droplet position is mildly affected by the fluid flow. (Right) Time evolution of deformation parameter D of the inner and the outer droplets.

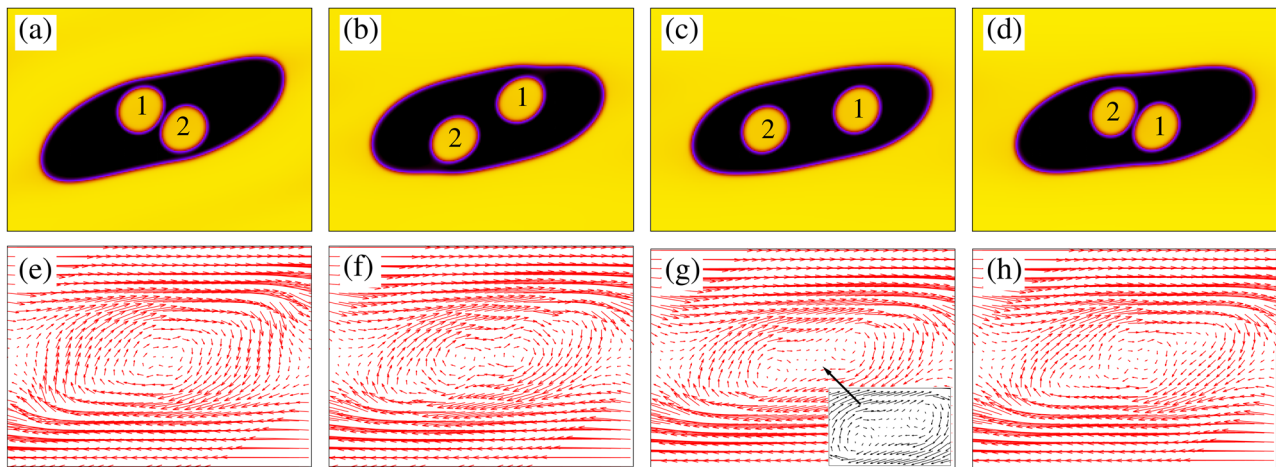


FIG. 7. [(a)–(d)] Steady state profiles of the fields ϕ_i of a two-droplet oscillatory dynamics under a symmetric shear flow with $\dot{\gamma} \simeq 3 \times 10^{-4}$. Snapshots are taken at (a) $t^* = 3$, (b) $t^* = 7.8$, (c) $t^* = 12$, and (d) $t^* = 18$. Here, $Re \simeq 2.6$ and $Ca \simeq 0.21$. [(e)–(h)] Steady state velocity profiles under shear. [Inset of (g)] A zoomed-in view of the two weak recirculations rotating clockwise formed nearby the inner droplets. Multimedia view: <https://doi.org/10.1063/1.5134901.4>

precisely dedicated to investigate the rheology of such a system in the presence of low/moderate shear flows.

C. Higher complex states: Multiple emulsion

1. Nonequilibrium steady states

We first consider likely the simplest example of a multiple emulsion, namely, two collinear fluid droplets located symmetrically with respect to an axis, parallel to z , passing through the center of mass of a surrounding larger droplet [see Fig. 2(c)]. Despite its essential design, a nontrivial rheological behavior emerges when subject to a shear flow.

Once a moderate shear is switched on, the two inner cores acquire motion, initially proceeding along opposite directions [Figs. 7(a) and 7(b)] and, later on, rotating periodically clockwise around the center of mass of the outer droplet by following roughly elliptical orbits [Figs. 7(c) and 7(d), (Multimedia view)]. As in a typical periodic motion, internal droplets attain the minimum speed (local minima of green and magenta plots of Fig. 8)

at the points of inversion of motion, while the highest speed is achieved halfway (maxima and minima of red and blue plots of Fig. 8).

Such planetlike oscillatory motion, observed during the transient dynamics and persistently at the steady state, is primarily caused by the confined geometry in which the internal droplets are constrained to move and, likewise, by the purely droplet-droplet repulsive interaction (an effect captured by the term proportional to ϵ in the free energy) combined with a nontrivial structure of the internal velocity field. Indeed, unlike the double emulsion, it exhibits a large fluid recirculation near the interface of the external droplet and two temporary recirculations within the emulsion, appearing faraway when the droplets invert their motion and merging into a single one when they are sufficiently close to each other.

Intriguingly, this dynamics produces significant effects on the external droplet shape. Although, like in the double emulsion, the droplet elongates and aligns along the direction imposed by the shear, at the steady state, it shows periodic shape deformations characterized by local interfacial bumps, more intense when

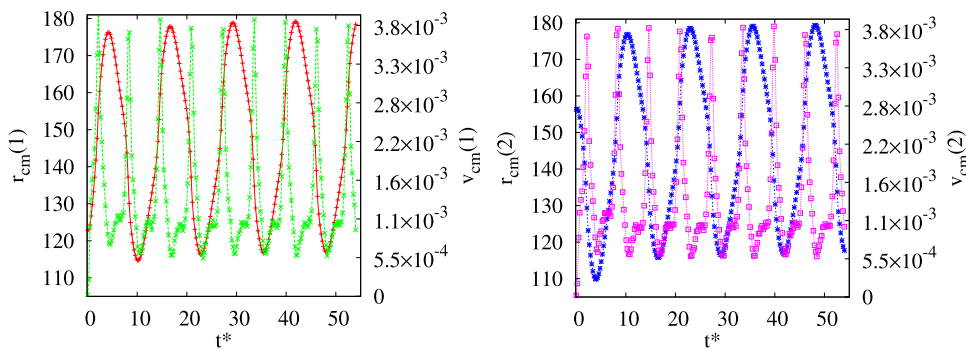


FIG. 8. Time evolution of the center of mass r_{cm} and of its speed v_{cm} when $\dot{\gamma} \simeq 3 \times 10^{-4}$ for droplet 1 (left) and droplet 2 (right) of Fig. 7. Red (pluses) and green (crosses) correspond, respectively, to the center of mass and speed of droplet 1, while blue (asterisks) and magenta (squares) correspond, respectively, to the center of mass and speed of droplet 2.

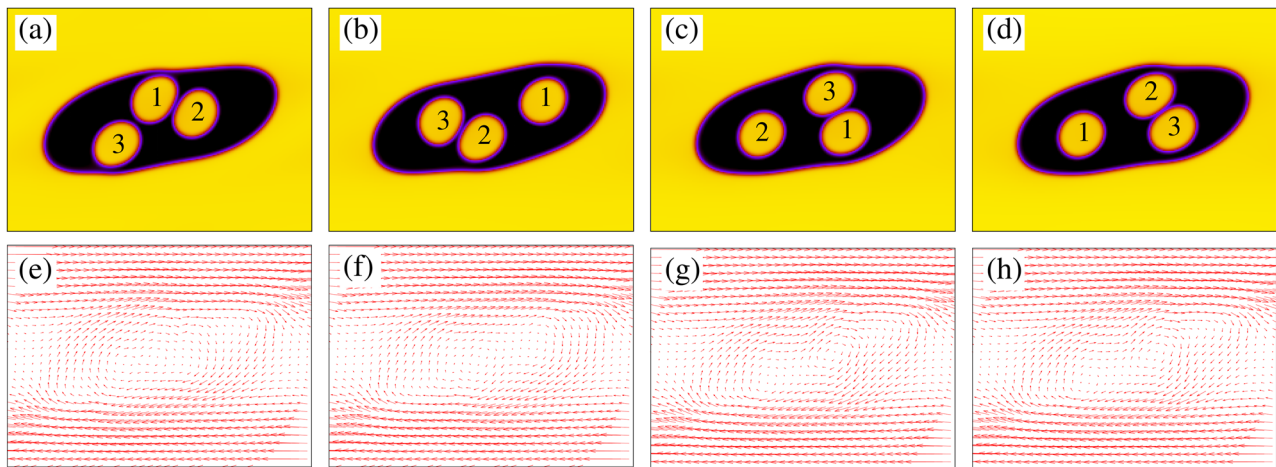


FIG. 9. [(a)–(d)] Steady state profiles of the fields ϕ_i of a three-droplet oscillatory dynamics emulsion under a symmetric shear flow with $\dot{\gamma} \approx 3 \times 10^{-4}$. Snapshots are taken at (a) $t^* = 6$, (b) $t^* = 12$, (c) $t^* = 18$, and (d) $t^* = 27$. Here, $Re \approx 6.6$ and $Ca \approx 0.52$. [(e)–(h)] Steady state velocity profiles under shear. Multimedia view: <https://doi.org/10.1063/1.5134901.5>

internal droplets approach the interface of the external one. When this occurs, the shape of the external droplet considerably departs from the typical ellipsoidal one observed in single and double emulsions, a geometry only temporarily restored when internal droplets are far from the external interface.

These results suggest a scenario in which (i) novel nonequilibrium steady states emerge whenever a multiple emulsion is subject to a shear flow and (ii) nontrivial deformations of the external interface emerge as a result of the internal droplets' motion. However, how robust is this dynamics? In addition, how does it depend on the arrangement of the internal droplets? Is the parameter D still a reliable quantity to capture droplet shape deformations even for moderate values of shear rates?

To partially address these questions, we study the dynamics under a moderate shear flow of a multiple emulsion in which three fluid droplets are encapsulated [see Fig. 2(d) for the initial condition]. The effect of the shear is overall similar to the previous case. During the transient dynamics, the external droplet elongates and stretches along the shear flow, while the internal ones acquire a clockwise rotating motion around the center of mass of the former.

At the steady state, such motion becomes, once again, periodic (see Fig. 9) (Multimedia view), with the internal droplets persistently moving along elliptical trajectories dragged by the large fluid recirculation formed near the external interface, where local deformations occur more frequently. Further weak fluid vortices also appear mainly located around the interface of the internal droplets. Hence, as long as $\dot{\gamma}$ is low enough to prevent the emulsion rupture, the periodic motion of the internal droplets is preserved, regardless of the droplets' arrangement. Even so, it is worth noting that increasing the number of internal droplets causes a sensible decrease in the tilt angle of the external droplet at the steady state. Indeed, we measure $\theta_o \approx 27^\circ$ for the two-core emulsion and $\theta_o \approx 18^\circ$ for the three-core one.

2. Interface deformation and stress tensor

An estimate of the shape deformation of the external droplet can be obtained by looking at the time evolution of parameter D . Interestingly, while for a single and a double emulsion, D rapidly attains a constant value, in a multiple emulsion, the periodic motion of the internal droplets leaves a tangible signature on it, which now displays periodic oscillations, more frequent as the number of the encapsulated droplets' augments (see Fig. 10). However, such behavior provides only partial knowledge about the correct shape of the external droplet, since it only captures a periodic elongation/contraction mechanism but misses the local interfacial bumps.

Further insights can be gained by computing the in plane component of the stress tensor Π_{yz} . Major contributions stem from the

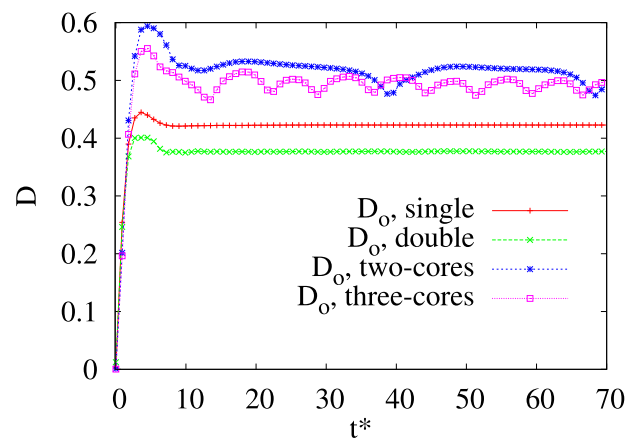


FIG. 10. Time evolution of the deformation D of the external droplet when $\dot{\gamma} \approx 4.5 \times 10^{-4}$. Periodic oscillations emerge when two and three droplets are included.

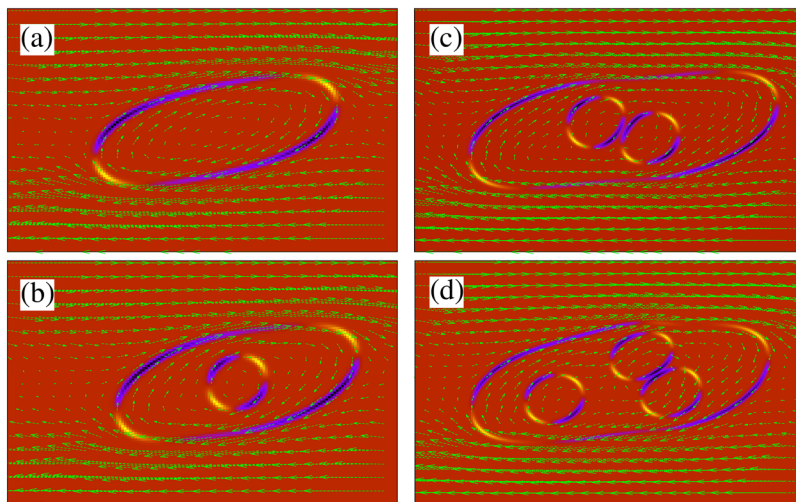


FIG. 11. Contour plot of Π_{yz} at the steady state for (a) isolated droplet, (b) double emulsion, (c) two-droplet monodisperse emulsion, and (d) three-droplet monodisperse emulsion. Color map ranges from 2×10^{-2} (yellow) to -2×10^{-2} (black). Negative values at the interface depend on the sign of derivative term in the stress tensor, proportional to $\partial_y \phi \partial_z \phi$. The arrows represent the velocity field of the fluid.

off diagonal term of Π_{yz}^{inter} and from the cross derivative terms of Π_{yz}^{visc} , proportional to $\partial_y v_z + \partial_z v_y$. The former is generally found to be more than one order of magnitude larger than the latter and is largely confined at the fluid interfaces of the external and internal droplets (see Fig. 11). Interestingly, the stress tensor exhibits a self-similar pattern, an indication that the coupling between fluid flow and interface deformations weakly depends on the number of internal droplets. These results suggest that the interfacial stress can describe the important aspects of the dynamics of the emulsion, such as periodic motion and interface deformations.

IV. CONCLUSIONS

To summarize, we have investigated the dynamics of a 2D multicore multiple emulsion under an imposed symmetric shear flow. We have kept the shear rate low enough to avoid the emulsion rupture but sufficiently intense to observe sizeable shape deformations. The physics of the steady states is crucially influenced by the shear rate and by the motion of the internal droplets. In the double emulsion, for instance, the latter undergoes shape deformations much weaker than the external one, which generally elongates until it attains an elliptical shape aligned with the shear flow, a behavior similar to that observed in an isolated single fluid droplet.

On the other hand, higher complex systems exhibit novel nonequilibrium steady states. If, for instance, two smaller droplets are dispersed in a large one, an oscillatory steady state is produced, in which the internal droplets periodically rotate around the center of mass of the latter. This dynamics is rather robust, since it occurs regardless of the initial droplet arrangement and at higher shear rates. In addition, for moderate values of the shear rate, marked local deformations are produced at the interface of the external droplets of a multiple emulsion, due to the dynamic interaction with the internal ones. This result suggests that, alongside the Taylor parameter D (a global quantity usually assumed to describe droplet deformations at low shear rates), further quantities, such as the stress tensor, may be necessary to accurately capture these local interfacial bendings.

Our analysis shows that the dynamics of multiple emulsions shows nontrivial qualitatively new phenomena as compared to the case of double emulsions, thereby raising a number of open questions.

Is there, for example, a feasible strategy favoring an alternative dynamic behavior of the internal droplets, keeping the shear rate at low/moderate values? A potential route worth exploring would be to increase the volume fraction of the internal droplets up to the close-packing limit to possibly trigger a chaoticlike dynamics. This point will be investigated in a future work.

Furthermore, a more careful control of the droplet deformation is experimentally achieved by either gelling or hardening the state of the fluid in the layer, an effect that could be modeled by releasing the approximation of single viscosity adopted for both fluid components. Deformations are also notably affected by the physics of the droplet-droplet repulsive interactions, whose structure is determined by the nature of surfactants. A weak surfactant, for example, may favor a partial droplet merging, an effect that could, in principle, be controlled by properly tuning the strength ϵ of the repulsive term. Even more intriguing would be the study of the effect produced by the simultaneous presence of different surfactants, whose physics can be modeled by allowing each phase field with its own repulsive strength $\epsilon(i)$.

Although still preliminary, we hope that our results may stimulate further experiments on multicore emulsions in microfluidic devices, which is of potential interest in applications relevant to drug delivery or in food processing.

SUPPLEMENTARY MATERIAL

See [supplementary material](#) for movie MS. It shows the dynamics of an isolated fluid droplet under symmetric shear for $\dot{\gamma} \sim 10^{-3}$.

ACKNOWLEDGMENTS

A.T., M.L., A.M., and S.S. acknowledge funding from the European Research Council under the European Union's Horizon 2020

TABLE I. Typical values of the physical quantities used in the simulations.

Model parameters	Simulation values	Physical values
Inner droplet radius, R_{in}	10	10 μm
Outer droplet radius, R_{out}	50	50 μm
Fluid viscosity, η	5/3	$\sim 10^{-2}$ Pa s
Surface tension, σ	0.08	~ 1 mN/m
Shear rate, $\dot{\gamma}$	10^{-4}	$\sim 0.02/\text{s}$

Framework Programme (No. FP/2014-2020) ERC Grant Agreement No. 739964 (COPMAT).

APPENDIX: MAPPING TO PHYSICAL UNITS

In Table I, we provide an approximate mapping between simulation parameters and real units. Parameters have been chosen in agreement with the values reported in previous simulation works, such as in Refs. 13, 62, and 63. Realistic values can be obtained by fixing the length scale, the time scale, and the force scale as $L = 1 \mu\text{m}$, $T = 10 \mu\text{s}$, and $F = 100 \text{ nN}$ (in simulations units, these scales are all equal to one), respectively.

REFERENCES

- K. J. Lissant, *Emulsions and Technology* (Marcel Dekker, New York, 1974), Vol. 6.
- A. Y. Kahn, S. Talegaonkar, Z. Iqbal, F. J. Ahmend, and R. K. Khar, "Multiple emulsions: An overview," *Curr. Drug Delivery* **3**, 4 (2006).
- S. S. Datta, A. Abbaspourrad, E. Amstad, J. Fan, S. H. Kim, M. Romanowsky, H. C. Shum, B. Sun, A. S. Utada, M. Windbergs, S. Zhou, and D. A. Weitz, "25th anniversary article: Double emulsion templated solid microcapsules: Mechanics and controlled release," *Adv. Mater.* **26**, 2205 (2014).
- G. T. Vladislavjevic, R. Al Nuamani, and S. A. Nabavi, "Microfluidic production of multiple emulsions," *Micromachines* **8**, 75 (2017).
- L. Y. Chu, A. S. Utada, R. K. Shah, J. W. Kim, and D. A. Weitz, "Controllable monodisperse multiple emulsions," *Angew. Chem., Int. Ed.* **46**, 8970 (2007).
- P. S. Clegg, J. W. Tavacoli, and P. J. Wilde, "One-step production of multiple emulsions: Microfluidic, polymer-stabilized and particle-stabilized approaches," *Soft Matter* **12**, 998 (2016).
- E. Dluska, A. Markowska-Radomska, A. Metera, B. Tudek, and K. Kosicki, "Multiple emulsions as effective platforms for controlled anti-cancer drug delivery," *Nanomedicine* **12**(18), 2183 (2017).
- M. Azarmanesh, S. Bawazeer, A. A. Mohamad, and A. Sanati-Nezhad, "Rapid and highly controlled generation of monodisperse multiple emulsions via a one-step hybrid microfluidic device," *Sci. Rep.* **9**, 12694 (2019).
- J. H. Xu, S. W. Li, J. Tan, Y. J. Wang, and G. S. Luo, "Controllable preparation of monodisperse O/W and W/O emulsions in the same microfluidic device," *Langmuir* **22**, 7943–7946 (2006).
- J. Santos, L. A. Trujillo-Cayado, N. Calero, M. C. Alfaro, and J. Munoz, "Development of eco-friendly emulsions produced by microfluidization technique," *J. Ind. Eng. Chem.* **36**, 90–95 (2016).
- S. Ding, C. A. Serra, T. F. Vandamme, W. Yu, and N. Anton, "Double emulsions prepared by two-step emulsification: History, state-of-the-art and perspective," *J. Controlled Release* **295**, 31 (2019).
- M. Azarmanesh, M. Farhadi, and P. Azizian, "Double emulsion formation through hierarchical flow-focusing microchannel," *Phys. Fluids* **28**, 032005 (2016).
- A. S. Utada, E. Lorenceau, D. R. Link, P. D. Kaplan, H. A. Stone, and D. A. Weitz, "Monodisperse double emulsions generated from a microcapillary device," *Science* **308**, 537–541 (2005).
- A. R. Abate and D. A. Weitz, "High-order multiple emulsions formed in poly(dimethylsiloxane) microfluidics," *Small* **5**, 2030–2032 (2009).
- L. D. Zarzar, V. Sresht, E. M. Sletten, J. A. Kalow, D. Blankschtein, and T. M. Swager, "Dynamically reconfigurable complex emulsions via tunable interfacial tensions," *Nature* **518**, 520–524 (2015).
- T. Y. Lee, T. M. Choi, T. S. Shim, R. A. Frijns, and S.-H. Kim, "Microfluidic production of multiple emulsions and functional microcapsules," *Lab Chip* **16**, 3415 (2016).
- S. Cohen, T. Yoshioka, M. Lucarelli, L. H. Hwang, and R. Langer, "Controlled delivery systems for proteins based on poly (lactic/glycolic acid) microspheres," *Pharm. Res.* **8**, 713–720 (1991).
- C. Laugel, P. Rafidison, G. Potard, L. Agudisch, and A. Baillet, "Modulated release of triterpenic compounds from a O/W/O multiple emulsion formulated with dimethicones: Infrared spectrophotometric and differential calorimetric approaches," *J. Controlled Release* **63**, 7–17 (2000).
- R. Cortesi, E. Esposito, G. Luca, and C. Nastruzzi, "Production of lipospheres as carriers for bioactive compounds," *Biomaterials* **23**, 2283–2294 (2002).
- A. Lamprecht, H. Yamamoto, H. Takeuchi, and Y. Kawashima, "pH-sensitive microsphere delivery increases oral bioavailability of calcitonin," *J. Controlled Release* **98**, 1–9 (2004).
- H. K. Kim and T. G. Park, "Comparative study on sustained release of human growth hormone from semi-crystalline poly (l-lactic acid) and amorphous poly (d,l-lactic-co-glycolic acid) microspheres: Morphological effect on protein release," *J. Controlled Release* **98**, 115–125 (2004).
- M. Maeki, *Microfluidics for Pharmaceutical Applications* (Elsevier, 2019), Chap. 4.
- H. Chen, Y. Zhao, Y. Song, and L. Jiang, "One-step multicomponent encapsulation by compound-fluidic electrospray," *J. Am. Chem. Soc.* **130**, 7800–7801 (2008).
- J. Lahann, "Recent progress in nano-biotechnology: Compartmentalized micro- and nanoparticles via electrohydrodynamic co-jetting," *Small* **7**, 1149–1156 (2011).
- C.-X. Zhao, "Multiphase flow microfluidics for the production of single or multiple emulsions for drug delivery," *Adv. Drug Delivery Rev.* **65**, 1420–1446 (2013).
- S. Kim, K. Kim, and S. Q. Choi, "Controllable one-step double emulsion formation via phase inversion," *Soft Matter* **14**, 1094 (2018).
- G. Muschiolik and E. Dickinson, "Double emulsions relevant to food systems: Preparation, stability, and applications," *Compr. Rev. Food Sci. Food Saf.* **16**, 532 (2017).
- W. Zhang, S. Zhao, W. Rao, J. Snyder, J. K. Choi, J. Wang, I. A. Khan, N. B. Saleh, P. J. Mohler, J. Yu, T. J. Hund, C. Tang, and X. He, "A novel core-shell microcapsule for encapsulation and 3D culture of embryonic stem cells," *J. Mater. Chem. B* **1**, 1002–1009 (2013).
- B. Cai, T.-T. Ji, N. Wang, X.-B. Li, R.-X. He, W. Liu, G. Wang, X.-Z. Zhao, L. Wang, and Z. Wang, "A microfluidic platform utilizing anchored water-in-oil-in-water double emulsions to create a niche for analyzing single non-adherent cells," *Lab Chip* **19**, 422 (2019).
- C.-H. Choi, H. Wang, H. Lee, J. H. Kim, L. Zhang, A. Mao, D. J. Mooney, and D. A. Weitz, "One-step generation of cell-laden microgels using double emulsion drops with a sacrificial ultra-thin oil shell," *Lab Chip* **16**, 1549 (2016).
- K. K. Brower, C. Carswell-Crumpton, S. Klemm, B. Cruz, G. Kim, S. G. K. Calhoun, L. Nichols, and P. M. Fordyce, e-print [bioRxiv:10.1101/803460v1](https://doi.org/10.1101/803460v1) (2019).
- N. N. Li and A. L. Shrier, "Liquid membrane water treating," *Recent Dev. Sep. Sci.* **1**, 163 (2018).
- F. Leal-Calderon, J. Bibette, and V. Schmitt, *Emulsion Science: Basic Principles* (Springer, 2007).
- V. Muguet, M. Seiller, G. Barratt, O. Ozer, J. P. Marty, and J. L. Grossiord, "Formulation of shear rate sensitive multiple emulsions," *J. Controlled Release* **70**, 37–49 (2001).
- M.-H. Lee, S.-G. Oh, S.-K. Moon, and S.-Y. Bae, "Preparation of silica particles encapsulating retinol using O/W/O multiple emulsions," *J. Colloid Interface Sci.* **240**, 83–89 (2001).

- ³⁶D.-H. Lee, Y.-M. Goh, J.-S. Kim, H.-K. Kim, H.-H. Kang, K.-D. Suh, and J.-W. Kim, "Effective formation of silicone-in-fluorocarbon-in-water double emulsions: Studies on droplet morphology and stability," *J. Dispersion Sci. Technol.* **23**, 491–497 (2002).
- ³⁷M. M. Rieger and L. D. Rhein, *Surfactants in Cosmetics* (Marcel Dekker Inc., New York, 2017).
- ³⁸S. Nafisi and H. Maibach, *Nanotechnology in Cosmetics* (Elsevier, 2017), Chap. 22.
- ³⁹A. Edris and B. Bergnsthäl, "Encapsulation of orange oil in a spray dried double emulsion," *Nahrung/Food* **45**, 133–137 (2001).
- ⁴⁰A. Benichou, A. Aserin, and N. Garti, "Double emulsions stabilized by new molecular recognition hybrids of natural polymers," *Polym. Adv. Technol.* **13**, 1019–1031 (2002).
- ⁴¹A. Benichou, A. Aserin, and N. Garti, "Double emulsions stabilized with hybrids of natural polymers for entrapment and slow release of active matters," *Adv. Colloid Interface Sci.* **108–109**, 29 (2004).
- ⁴²A. K. L. Oppermann, L. C. Verkaik, M. Stieger, and E. Scholten, "Influence of double ($w_1/o/w_2$) emulsion composition on lubrication properties," *Food Funct.* **8**, 522 (2017).
- ⁴³S. Omi, K. Katami, T. Taguchi, K. Kaneko, and M. Iso, "Synthesis of uniform pmma microspheres employing modified SPG (shirasu porous glass) emulsification technique," *J. Appl. Polym. Sci.* **57**, 1013 (2003).
- ⁴⁴L. Y. Chu, R. Xie, J. H. Zhu, W. M. Chen, T. Yamaguchi, and S. I. Nakao, "Study of SPG membrane emulsification processes for the preparation of monodisperse core-shell microcapsules," *J. Colloid Interface Sci.* **265**, 187 (2003).
- ⁴⁵R. Alex and R. Bodmeier, "Encapsulation of water-soluble drugs by a modified solvent evaporation method. I. effect of process and formulation variables on drug entrapment," *J. Microencapsulation* **7**, 347 (1990).
- ⁴⁶S.-H. Kim and D. A. Weitz, "One-step emulsification of multiple concentric shells with capillary microfluidic devices," *Angew. Chem., Int. Ed.* **50**, 8731–8734 (2011).
- ⁴⁷X. C. i. Solvas and A. deMello, "Droplet microfluidics: Recent developments and future applications," *Chem. Commun.* **47**, 1936–1942 (2011).
- ⁴⁸D. Saeki, S. Sugiura, T. Kanamori, S. Sato, and S. Ichikawa, "Microfluidic preparation of water-in-oil-in-water emulsions with an ultra-thin oil phase layer," *Lab Chip* **10**, 357 (2010).
- ⁴⁹B. Dollet, A. Scagliarini, and M. Sbragaglia, "Two-dimensional plastic flow of foams and emulsions in a channel: Experiments and lattice Boltzmann simulations," *J. Fluid Mech.* **766**, 556 (2015).
- ⁵⁰L. Derzsi, D. Filippi, G. Mistura, M. Pierno, M. Lulli, M. Sbragaglia, M. Bernaschi, and P. Garstecki, "Fluidization and wall slip of soft glassy materials by controlled surface roughness," *Phys. Rev. E* **95**, 052602 (2017).
- ⁵¹M. Lulli, R. Benzi, and M. Sbragaglia, "Metastability at the yield-stress transition in soft glasses," *Phys. Rev. X* **8**, 021031 (2018).
- ⁵²F. Pelusi, M. Sbragaglia, and R. Benzi, "Avalanche statistics during coarsening dynamics," *Soft Matter* **15**, 4518 (2019).
- ⁵³X. Chen, Y. Liu, and M. Shi, "Hydrodynamics of double emulsion droplet in shear flow," *Appl. Phys. Lett.* **102**, 051609 (2013).
- ⁵⁴Y. Chen, X. Liu, and Y. Zhao, "Deformation dynamics of double emulsion droplet under shear," *Appl. Phys. Lett.* **106**, 141601 (2015).
- ⁵⁵Y. Chen, L. Xiangdong, Z. Chengbin, and Z. Yuanjin, "Enhancing and suppressing effects of an inner droplet on deformation of a double emulsion droplet under shear," *Lab Chip* **15**, 1255–1261 (2015).
- ⁵⁶H. A. Stone and L. G. Leal, "Breakup of concentric double emulsion droplets in linear flows," *J. Fluid Mech.* **211**, 123–156 (1990).
- ⁵⁷Y. Y. Renardy and V. Cristini, "Effect of inertia on drop breakup under shear," *Phys. Fluids* **13**, 7 (2001).
- ⁵⁸S. Afkami, P. Yue, and Y. Renardy, "A comparison of viscoelastic stress wakes for two-dimensional and three-dimensional Newtonian drop deformations in a viscoelastic matrix under shear," *Phys. Fluids* **21**, 072106 (2009).
- ⁵⁹J. W. Ha and S. M. Yang, "Fluid dynamics of a double emulsion droplet in an electric field," *Phys. Fluids* **11**, 1029 (1999).
- ⁶⁰J. Wang, J. Liu, J. Han, and J. Guan, "Effects of complex internal structures on rheology of multiple emulsions particles in 2D from a boundary integral method," *Phys. Rev. Lett.* **110**, 066001 (2013).
- ⁶¹K. A. Smith, J. M. Ottino, and M. O. de la Cruz, "Encapsulated drop breakup in shear flow," *Phys. Rev. Lett.* **93**, 204501 (2004).
- ⁶²M. Fogliano, A. N. Morozov, O. Henrich, and D. Marenduzzo, "Flow of deformable droplets: Discontinuous shear thinning and velocity oscillations," *Phys. Rev. Lett.* **119**, 208002 (2017).
- ⁶³M. Fogliano, A. N. Morozov, and D. Marenduzzo, "Rheology and microrheology of deformable droplet suspensions," *Soft Matter* **14**, 9361 (2018).
- ⁶⁴S. R. De Groot and P. Mazur, *Non-Equilibrium Thermodynamics* (Dover, New York, NY, 1984).
- ⁶⁵R. Mueller, J. M. Yeomans, and A. Doostmohammadi, "Emergence of active nematic behavior in monolayers of isotropic cells," *Phys. Rev. Lett.* **122**, 048004 (2019).
- ⁶⁶V. M. Kendon, M. E. Cates, I. Pagonabarraga, J. C. Desplat, and P. Blandon, "Inertial effects in three-dimensional spinodal decomposition of a symmetric binary fluid mixture: A lattice Boltzmann study," *J. Fluid Mech.* **440**, 147–203 (2001).
- ⁶⁷T. Krüger, H. Kusumaatmaja, A. Kuzmin, O. Shardt, G. Silva, and E. M. Viggien, *The Lattice Boltzmann Method* (Springer International Publishing, 2017), Vol. 10, pp. 978–983.
- ⁶⁸S. Succi, *The Lattice Boltzmann Equation: For Complex States of Flowing Matter* (Oxford University Press, 2018).
- ⁶⁹R. Benzi, S. Succi, and M. Vergassola, "The lattice Boltzmann equation: Theory and applications," *Phys. Rep.* **222**, 145–197 (1992).
- ⁷⁰M. R. Swift, E. Orlandini, W. R. Osborn, and J. M. Yeomans, "Lattice Boltzmann simulations of liquid-gas and binary fluid systems," *Phys. Rev. E* **54**, 5041 (1996).
- ⁷¹M. Bernaschi, S. Melchionna, and S. Succi, "Mesoscopic simulations at the physics-chemistry-biology interface," *Rev. Mod. Phys.* **91**, 025004 (2019).
- ⁷²A. Montessori, M. Lauricella, N. Tirelli, and S. Succi, "Mesoscale modelling of near-contact interactions for complex flowing interfaces," *J. Fluid Mech.* **872**, 327 (2019).
- ⁷³S. Ansumali and I. V. Karlin, "Kinetic boundary conditions in the lattice Boltzmann method," *Phys. Rev. E* **66**, 026311 (2002).
- ⁷⁴S. Ansumali, I. V. Karlin, S. Arcidiacono, S. Abbas, and N. I. Prasianakis, "Hydrodynamics beyond Navier-Stokes: Exact solution to the lattice Boltzmann hierarchy," *Phys. Rev. Lett.* **98**, 124502 (2007).
- ⁷⁵A. Tiribocchi, N. Stella, G. Gonnella, and A. Lamura, "Hybrid lattice Boltzmann model for binary fluid mixtures," *Phys. Rev. E* **80**, 026701 (2009).
- ⁷⁶G. Gonnella, A. Lamura, A. Piscitelli, and A. Tiribocchi, "Phase separation of binary fluids with dynamic temperature," *Phys. Rev. E* **82**, 046302 (2010).
- ⁷⁷G. Falcucci, S. Ubertini, C. Biscarini, S. Di Francesco, D. Chiappini, S. Palpacelli, A. De Maio, and S. Succi, "Lattice Boltzmann methods for multiphase flow simulations across scales," *Commun. Comput. Phys.* **9**, 269 (2015).
- ⁷⁸Y. Gan, A. Xu, G. Zhang, and S. Succi, "Discrete Boltzmann modeling of multiphase flows: Hydrodynamic and thermodynamic non-equilibrium effects," *Soft Matter* **11**, 5336 (2015).
- ⁷⁹C. Denniston, D. Marenduzzo, E. Orlandini, and J. M. Yeomans, "Lattice Boltzmann algorithm for three-dimensional liquid-crystal hydrodynamics," *Philos. Trans. R. Soc., A* **362**, 1745–1754 (2004).
- ⁸⁰T. A. Wood, J. S. Lintuvuori, A. B. Schofield, D. Marenduzzo, and W. C. K. Poon, "A self-quenched defect glass in a colloid-nematic liquid crystal composite," *Science* **334**, 79–83 (2011).
- ⁸¹A. Tiribocchi, O. Henrich, J. S. Lintuvuori, and D. Marenduzzo, "Switching hydrodynamics in liquid crystal devices: A simulation perspective," *Soft Matter* **10**, 4580–4592 (2014).
- ⁸²G. Foffano, J. S. Lintuvuori, A. Tiribocchi, and D. Marenduzzo, "The dynamics of colloidal intrusions in liquid crystals: A simulation perspective," *Liq. Cryst. Rev.* **2**, 1–27 (2014).
- ⁸³A. Tiribocchi, M. Da Re, D. Marenduzzo, and E. Orlandini, "Shear dynamics of an inverted nematic emulsion," *Soft Matter* **12**, 8195–8213 (2016).
- ⁸⁴M. E. Cates, O. Henrich, D. Marenduzzo, and K. Stratford, "Lattice Boltzmann simulations of liquid crystalline fluids: Active gels and blue phases," *Soft Matter* **5**, 3791–3800 (2009).

⁸⁵L. N. Carenza, G. Gonnella, A. Lamura, G. Negro, and A. Tiribocchi, “Lattice Boltzmann methods and active fluids,” *Eur. Phys. J. E* **42**, 81 (2019).

⁸⁶B. J. Bentley and L. G. Leal, “An experimental investigation of drop deformation and breakup in steady, two-dimensional linear flows,” *J. Fluid Mech.* **167**, 241–283 (1986).

⁸⁷S. Zaleski, J. Li, and S. Succi, “Two dimensional Navier-Stokes simulation of deformation and breakup of liquid patches,” *Phys. Rev. Lett.* **75**, 244 (1995).

⁸⁸J. M. Rallison, “The deformation of small viscous drops and bubbles in shear flows,” *Annu. Rev. Fluid Mech.* **16**, 45–66 (1984).

⁸⁹F. S. Hakimi and W. R. Schowalter, “The effects of shear and vorticity on deformation of a drop,” *J. Fluid Mech.* **98**, 635–645 (1980).